Distant homologies and domain conservation of the Hereditary Spastic Paraplegia protein SPG11/ALS5/spatacsin

Alexander L Patto and Cahir J O'Kane*

Department of Genetics, University of Cambridge, Downing Street, Cambridge, CB2 3EH

*Corresponding author Email: c.okane@gen.cam.ac.uk

Abstract

Loss-of-function mutations in SPG11 protein (spatacsin) are a common cause of autosomal recessive hereditary spastic paraplegia with thin corpus callosum. To identify regions of the protein that may have functions that are disrupted in disease, we carried out bioinformatic analyses of its conserved regions. An N-terminal region of around 650 amino-acid residues, present in SPG11 across a wide range of metazoan animals, was missing from many insect lineages. Evolutionary loss of this domain correlated with loss of its binding partner, the AP-5 adaptor complex, suggesting that its main function is interaction with AP-5 in intracellular trafficking, and that the remainder of SPG11 carries out AP-5-independent functions. At the C-terminus of SPG11, a spatacsin_C domain showed sequence similarity and predicted structural homology to the Vps16_C domain of the HOPS complex protein Vps16. It localized partly to acidic compartments, consistent with a role in endolysosomal or autolysosomal transport, like Vps16. Mass spectrometry analysis of binding partners of this domain identified actin cytoskeletal and proteasome proteins, some SM proteins, and a number of aminoacyl-tRNA synthetases. Since mutations affecting SPG11 or aminoacyl-tRNA synthetases can cause Charcot-Marie-Tooth neuropathy (CMT), we suggest autolysosomal trafficking, and in particular autophagic lysosome reformation, as a target process in CMT.

Introduction

Loss-of-function mutations in *SPG11* commonly result in autosomal recessive Hereditary Spastic Paraplegia (ARHSP) with thinning of the corpus callosum (TCC) (Stevanin et al., 2007). *SPG11* is the most common recessive HSP, with HSP-causing mutations identified throughout the coding region. *SPG11* mutations can also cause other degenerative disorders including juvenile ALS (Daoud et al., 2012; Orlacchio et al., 2010), juvenile Parkinson's disease and dopaminergic neuron loss (Anheim et al., 2009; Guidubaldi et al., 2011), Kjelllin's syndrome, or the peripheral neuropathy Charcot-Marie-Tooth disease (Fridman and Murphy, 2014; Montecchiani et al., 2016).

Loss of *SPG11* in mammals leads to axonal pathology, including axonal outgrowth defects in mouse (Pérez-Brangulí et al., 2014). Young *Spg11* knockout mice have severe neuronal loss in the cerebellum, motor cortex and Purkinje cells (Varga et al., 2015). Externally, mice develop a progressive gait disorder, present with ataxia after 12 months (Varga et al., 2015), consistent with symptoms in *SPG11* patients (Zhao et al., 2013). In zebrafish, severe knockdown of *Spg11* or *Spg15* led to similar defects in spinal motor neuron axon outgrowth and locomotion diculties (Martin et al., 2012). *Spg11* phenotypes in animal models are broadly consistent with human *SPG11* phenotypes, suggesting important roles for SPG11 in neuronal development and function.

SPG11 localizes to Lamp1-positive compartments in human fibroblasts (Hirst et al., 2013), which comprise lysosomes (Rohrer et al., 1996), autolysosomes (Yu et al., 2010) and late endosomes (Szymanski et al., 2011). SP11 and its binding partner SPG15 interact with the adaptor protein complex AP-5 (Hirst et al., 2011; Renvoisé et al., 2014; Słabicki et al., 2010), by binding of the SPG11 N-terminus to AP-5 (Hirst et al., 2013). SPG11 and SPG15 depend on each other for localization (Hirst et al., 2013), and knockdown of either disrupts AP-5 localisation; conversely, knockdown of *AP5z1* has no effect on the localisation of SPG11 or SPG15 (Hirst et al., 2013). SPG11 and SPG15 show structural homology with clathrin heavy chain and COP1 subunits (Hirst et al., 2011; Hirst et al., 2013); however, they are not recruited by an AP-5 adaptor. Loss of SPG11, SPG15 or the AP-5 subunit AP5z1 causes accumulation of the mannose 6-phosphate receptor (CIMPR) in early endosomes (Hirst et al., 2013), and proteomic analyses of of AP5z1 knockout cells suggest a defect in transport from late endosomes to the Golgi (Hirst et al., 2018). Therefore, SPG11, SPG15 and AP-5 appear to share trafficking roles that may be disrupted in HSP.

However, SPG11 must also have AP-5-independent roles, which may account for disease phenotypes like ALS, PD or CMT, that are not so far found in human AP-5 mutant genotypes.

Mutations in *AP5z1* are associated with hereditary spastic paraplegia, although protein null alleles appear in general to have later onset (Hirst et al., 2016; Słabicki et al., 2010) than *SPG11* or *SPG15* (Boukhris et al., 2008; Pensato et al., 2014; Stevanin et al., 2007). Further, *Drosophila* contains both SPG11 and SPG15 homologs, but lacks AP-5 (Hirst et al., 2011). Such an AP-5-independent role appears to be in autophagic lysosome reformation (ALR) (Chang et al., 2014; Varga et al., 2015), which replenishes free lysosomes after periods of increased autophagy (Yu et al., 2010). Loss of SPG11 or SPG15 results in enlarged or excess autolysosomes, and loss of Lamp1-positive tubules on autolysosomes, thought to be an intermediate in ALR (Chang et al., 2014; Vantaggiato et al., 2013; Varga et al., 2015). Levels of LC3-II, an indicator of autophagy flux (Mauvezin et al., 2014), increase, but not Lamp1, suggesting aberrant lysosome-dependent clearance of autophagosomes (Chang et al., 2014; Varga et al., 2015)]. *Spg11* knock-out mice display fewer free lysosomes in Purkinje cell somata (Varga et al., 2015), consistent with impaired ALR *in vivo*. Mutant *SPG15* patient fibroblasts accumulate autophagy substrate p62 (Vantaggiato et al., 2013), and *SPG11* knock-out Purkinje cells show increased p62 in Lamp1-positive compartments, suggesting that autolysosomes are not completely functional (Varga et al., 2015). *SPG11* knock-out mice have severe neuronal degeneration, with mice developing a progressive gait disorder and ataxia (Varga et al., 2015). The above findings suggest a key role for SPG11 in ALR, and that ensuing accumulation of undegraded material in the absence of SPG11 may be a cause of neuronal degeneration (Varga et al., 2015).

However, the molecular role of SPG11 in autophagic trafficking, the steps it affects, and the nature of its AP-5- independent function are not clear. To identify potential roles for SPG11 in this process, we undertook bioinformatic analyses of the protein. We found that the presence or absence of the N-terminal region, found in most metazoan lineages, correlates with the presence or absence of the AP-5 adaptor complex, suggesting that the main function of the N-terminal region is to interact with AP-5. We also found evidence that the spatacsin_C domain at the C-terminus of SPG11 is homologous to the Vps16_C domain, and identified binding partners that suggest related mechanisms for CMT pathology between SPG11 and aminoacyl-tRNA synthetases.

Results

N-terminal AP-5-binding region of SPG11 is absent in insect lineages. We used bioinformatic tools to identify potential functional domains within SPG11. Multiple alignments have shown extensive conservation along the length of SPG11 proteins, but with no identifiable domains of known function (Hirst et al., 2011; Hirst et al., 2013). The best characterized molecular function lies in a predicted beta-propeller-like fold in the N-terminal 500 amino-acid residues of human SPG11, which interacts with the AP-5 adaptor (Hirst et al., 2013). Using Kalign multiple alignment (Lassmann and Sonnhammer, 2005), we found that all deuterostomes aligned possess this region (Figure 1), and many protostomes, including arachnids, molluscs, annelids and brachiopods. However, *Drosophila* and other insects lack approximately 650 amino acids from the N-terminus of SPG11 (known as CG13531 in *Drosophila*), which contains the AP-5-binding domain (Figure 1).

AP-5 is an ancient adaptor complex, but has frequently been lost during eukaryote evolution. To test whether its loss correlates with loss of the SPG11 N-terminus, we tested a range of metazoans for the presence of any of the four AP-5 subunits (Hirst et al., 2011). AP-5 is present in basal animal phyla such as *Cnidaria*, the sponge *Amphimedon*, and the Placozoan *Trichoplax*; it is also found widely in deuterostomes (Figs S1-S4). In protostomes, it is found in molluscs (*Octopus*, *Lottia, Crassostrea, Biomphalaria*), the brachiopod *Lingula*, the annelid *Capitella*, the priapulid worm *Priapulus*, and some arthropods (*Limulus*, *Parasteatoda*), but not in insects. Most organisms that lack the SPG11 N-terminal region (Figure 1) also lack AP-5 (Figs S1-S4), suggesting that the primary role of the N-terminus of SPG11 is to bind AP-5.

In a few species, we found an SPG11 N-terminal domain, but not AP-5: the arthropods *Sarcoptes* and *Metaseiulus*, and the mollusc *Aplysia* (Figure 1). However, the arthropods most closely related to *Sarcoptes* and *Metaseiulus* (*Limulus*, *Parasteatoda*), and other molluscs (*Octopus*, *Lottia*), possess both AP-5 and the SPG11 N-terminus, suggesting either that AP-5 in *Sarcoptes*, *Metaseiulus* and *Aplysia* has not yet been annotated, or they have lost AP-5 relatively recently, but not yet the SPG11 N-terminus.

SPG11 C-terminus has predicted homology with the Vps33-binding domain of Vps16. Human and *Drosophila* SPG11 share 16% identity across the entire protein sequence, with a region of around 300 amino acid residues with higher identity (31%) at the C-terminus (Figure 2A). This region is designated as a Spatacsin_C domain (Pfam 14649; Interpro IPR028107), but its function or structure is unknown. To identify domains homologous to this region of

Fig. 1

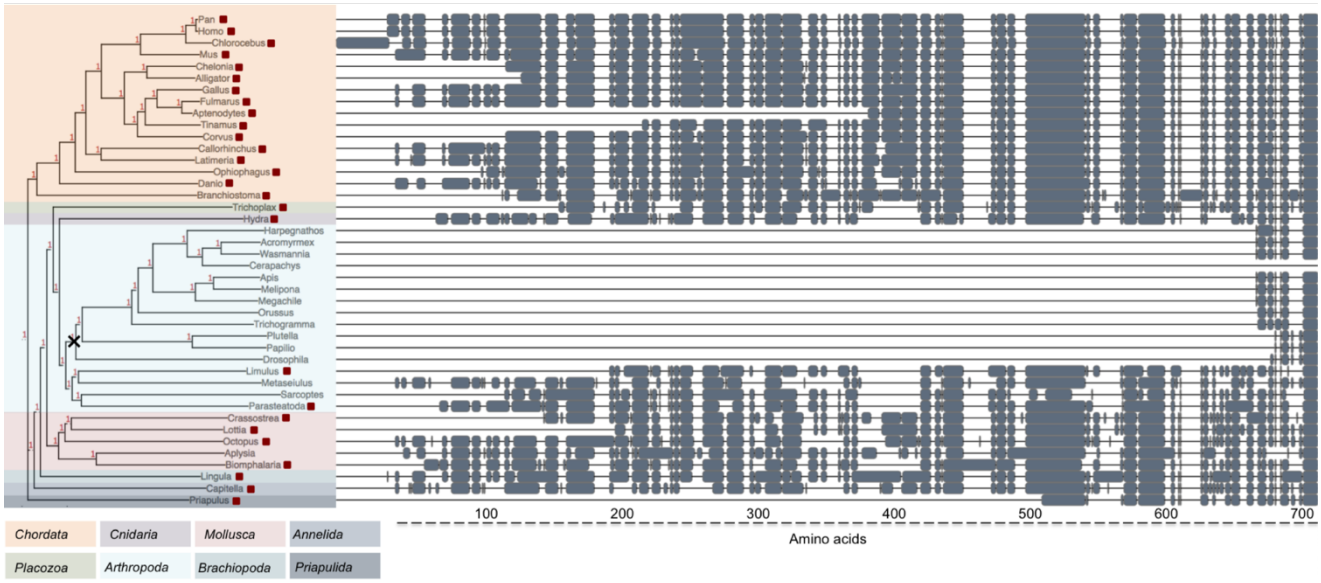

Fig. 1. SPG11 phylogenetic tree across a range of metazoans. Left: Phylogenetic tree of SPG11 amino acid sequence, made using Kalign multiple alignment (Lassmann and Sonnhammer, 2005). Organisms containing AP-5 (Figs S1-S4) are shown by red squares. Shaded regions denote different phyla. Right: A condensed overview of aligned SPG11 N-terminal regions, created using online tree viewer (http://etetoolkit.org/treeview/). Predicted loss of N-terminal region occurs prior to the emergence of insects (cross).

SPG11, we used both the *Drosophila* and human sequenecs as queries in HH-pred searches, which can identify distant homologies between proteins using the Structural Classification of Proteins database (SCOP) (Söding et al., 2005). HH-pred previously predicted a beta-propeller-like region in the N-terminal AP-5-binding domain (Hirst et al., 2013); it also predicts homology of some regions of *Drosophila* SPG11 to coatomer subunits, as previously predicted for human SPG11 (Figure 2B). At the C-terminus, HH-pred predicted homology to features of the Vps33-Vps16 HOPS subcomplex (PDB - 10.2210/pdb4kmo/pdb) in both human and fly SPG11, across most of the C-terminal 300 amino acid residues (Figure 2B,C). The Vps33-Vps16 subcomplex contains the C-terminal region of Vps16 (Vps16_C, Pfam ID: PF04840) which recruits the SM protein Vps33 [177] (Baker et al., 2013; Graham et al., 2013), and HH-Pred also predicts homology to Vps16 itself. Taken together, this suggests that SPG11 C-terminus has homology with the Vps16_C domain.

We further tested homology between the SPG11 C-terminus and the Vps16_C domain by alignment of several Vps16_C and SPG11 C-terminus sequences. This showed extensive similarity between the two sequences, with idential or conserved amino acid residues at many positions (Figure 3A). However, many known Vps33-binding residues of the Vps16_C domain of Vps16 (Baker et al., 2013; Graham et al., 2013) were either missing or not conserved in SPG11 (Figure 3A). Together these results support homology of the SPG11 C-terminal domain to Vps16_C, but do not strongly support binding to Vps33.

SPG11 C-terminus predicted tertiary structure similar to Vps16_C. We assessed whether the SPG11 C-teminus might have a similar structure to Vps16, using tertiary structure prediction software. Vps16_C forms an alpha-solenoid domain with 17 alpha-helices (Baker et al., 2013; Graham et al., 2013). Vps16_C binds to all 3 domains present in Vps33, and thus arches around Vps33, with the N-terminal region of Vps16_C lying in the groove between domain 1 and 2 of Vps33 (Baker et al., 2013; Graham et al., 2013). We used the *Drosophila* SPG11 C-terminus (amino acids 1496-1815) as an input query using iTASSER tertiary prediction software (Yang et al., 2014). iTASSER predicts tertiary structure by aligning the input query with templates from known protein structures from PDB. The top hit identified was the crystal structure of Vps16_C in the Vps33-Vps16 HOPS subcomplex (10.2210/pdb4kmo/pdb) (Figure 3B). The TM-score was 0.93; this is a metric for the structural similarity of two protein models, with a value of 1 being identical structures (Yang et al., 2014).

Fig. 2

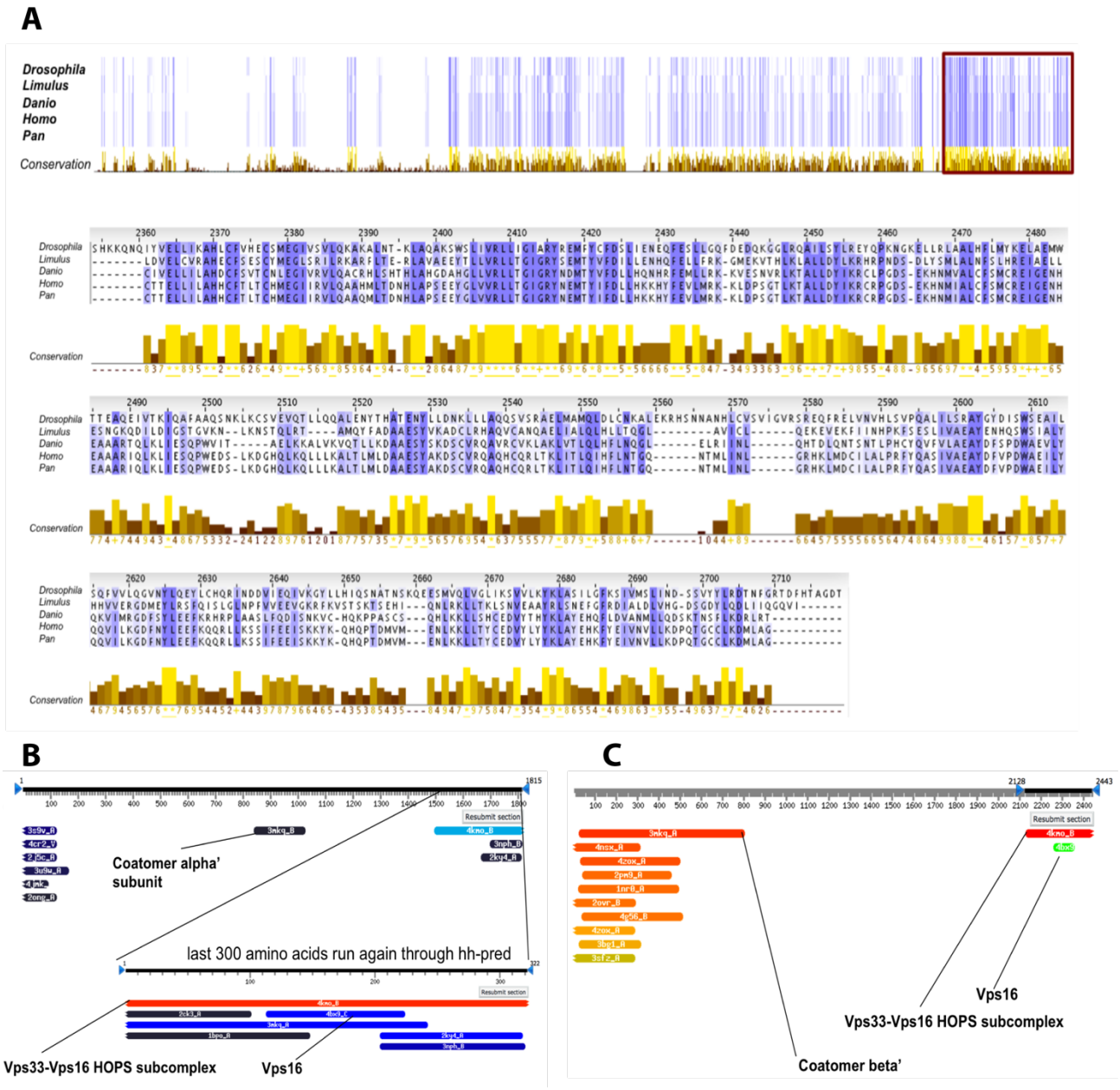

Fig. 2. Sequence conservation across the length of Spg11. A. MUSCLE multiple alignment of SPG11 from *D. melanogaster*, *L. polyphemus*, *D. rerio*, *H. sapiens* and *P. troglodytes*, shown in Jalview. Top panel: blue shaded regions show regions of amino acid identity between organisms; intensity of blue corresponds with level of identity. Yellow bars at the bottom denote conservation level between organisms for individual amino acid positions. Red box indicates SPG11 C-terminal region with high conservation. This region is expanded in the lower panels to show conservation and alignment of amino acid sequences. **B:** HH-pred of *Drosophila* SPG11 predicts coatomer homology in the central region of the proteins, and homology to Vps33-Vps16 HOPS subcomplex and Vps16 in the C-terminal region. **C:** HH-pred of human SPG11 predicts extended homology to coatomer beta' subunit at the N-terminus and to Vps33-Vps16 HOPS subcomplex and Vps16 at the C-terminus.

Fig. 3

A

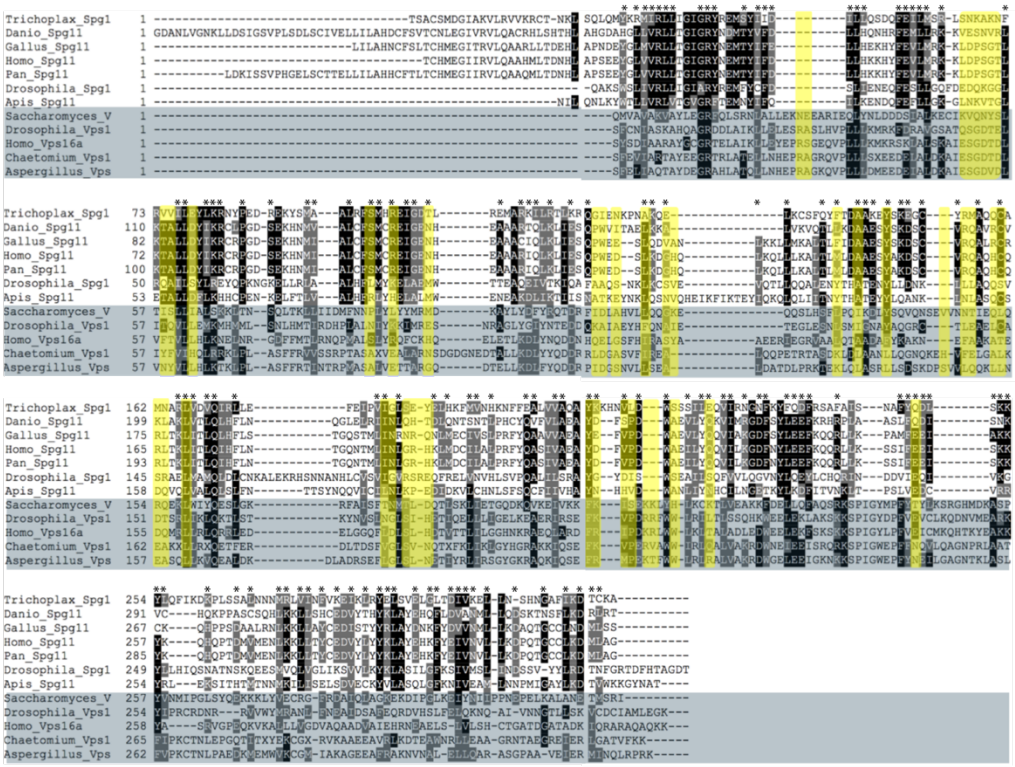

B

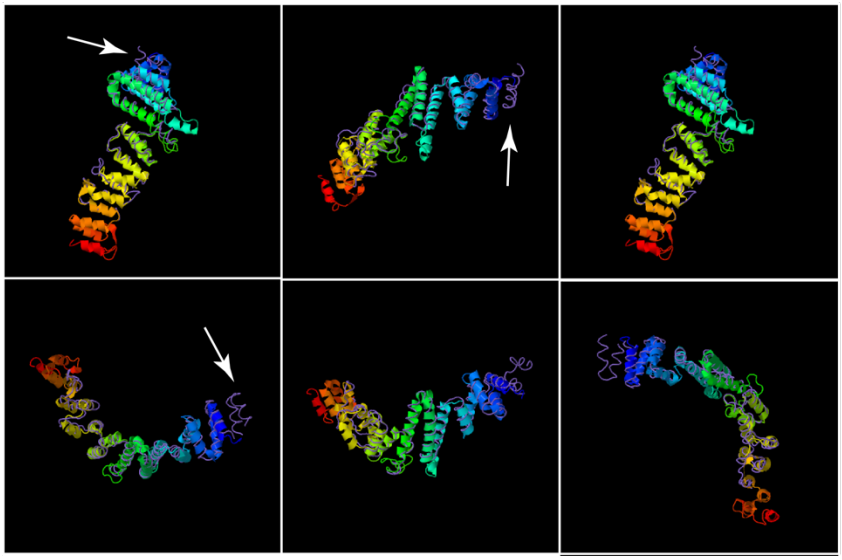

Fig. 3. SPG11 C-terminus has homology with Vps16_C. A. Multiple alignment of seven Spg11 C-terminal sequences and five Vps16_C sequences, created using MUSCLE. Residues shaded in black and gray show highest conservation. Asterisks show residues that are mostly identical or conserved across both Spg11 and Vps16_C sequences. Yellow shaded regions denote Vps33-binding regions in Vps16a (Baker et al., 2013; Graham et al., 2013). **B.** iTASSER tertiary prediction of Spg11 C-teminus. Rainbow protein fold represents predicted Spg11_C structure. Overlaid is the known Vps16_C known tertiary structure in purple (arrow). Panels display the predicted structure from different angles.

GFP-tagged SGP11 C-terminus overlaps with acidic compartments. To investigate whether a GFP-tagged Drosophila SPG11 C-terminus, GFP::Spg11-C (amino acid residues 1468-1815) expressed in *Drosophila* Mel-2 cells was possibly functional, we tested whether it localized to endo/auto/lysosomal compartments like Vps16 (Kim et al., 2001; Schröder et al., 2007; Wartosch et al., 2015) and Spg11 (Hirst et al., 2012; Murmu et al., 2011; Varga et al., 2015) localised to similar structures as Spg11::GFP. As predicted, GFP::Spg11-C localised partly to LysoTracker®-positive compartments (Figure 4A).

Identification of SPG11 C-terminus binding partners by mass spectrometry. To test further the functionality of the SPG11 C-terminus, we expressed GFP-tagged *Drosophila* SPG11 C-terminal domain in *Drosophila* Mel-2 cells, to conduct mass spectrometry analysis. We established two cell lines: one in which GFP::Spg11-C was driven by a constitutively active promoter (Act5-GFP::Spg11-C) and one driven by a $CuSO_4$-inducible promoter (PMT-GFP::Spg11-C). A Mel-2 cell line expressing GFP (inducible by $CuSO_4$) was used as a negative control.

Mass spectrometry analysis of purified GFP::Spg11-C from the $CuSO_4$-induced cels identified 898 proteins that were not found in the GFP negative control, whereas analysis of constitutively expressed GFP::Spg11-C only identified 231 proteins; the top 100 hits from each analysis are listed in Tables 1 and 2. The $CuSO_4$-induced cells generated many protein hits that were higher scoring than the same protein in the control cell line, compared to the constitutive cells (Figure 5B). Taken together, this suggests that GFP::Spg11-C was more highly expressed in the $CuSO_4$-inducible cell line than the constitutive one. 128 proteins were detected in both lines (Table 3), providing increased confidence in the specificity of these interactors, although this overlapping list will be missing some genuine interactors identified in the $CuSO_4$-induced cells.

Binding partners of purified GFP::Spg11-C. GFP::Spg11-C was detected in both expression lines, and was absent in the GFP negative control, confirming that GFP::Spg11-C is expressed, and that the mass spectrometry protocol worked (Figure 5B); it was the highest scoring hit in the $CuSO_4$-induced line, but not in the constitutively expressing cell line (Figure 5B). Reassuringly, the SPG11 binding partner, SPG15, was identified in the inducible cell line, although not in the constitutive one. Other binding partners were enriched for proteasome components and the actin cytoskeleton (Table 4; Fig. 6). We also noticed several membrane-traffic related proteins, and motor proteins of the kinesin, dynein and myosin families (Tables 1-3, entries in bold; Fig. 6).

Fig. 4

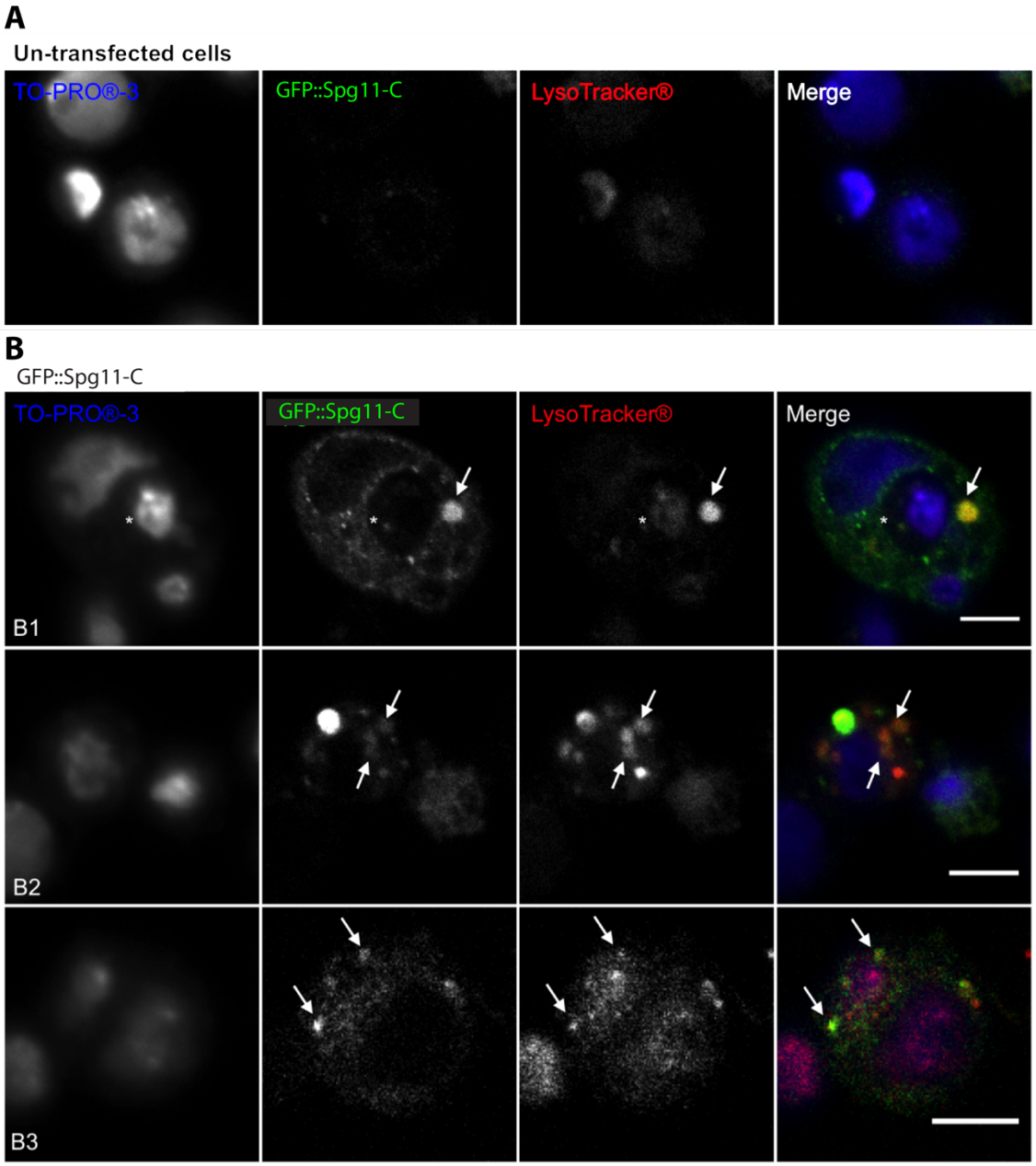

Fig. 4. Localisation of GFP::Spg11-C in *Drosophila* Dmel-2 cells. A: Untransfected cells, used as a negative control display no GFP signal; brightness is adjusted to twice that of experimental panels, to show lack of signal in GFP channel (second panel from left). **B:** GFP-tagged Spg11 C-terminus (GFP::Spg11-C) did not localise to the nuclear stain TOPRO-3 (B1, asterisk). Many GFP::Spg11-C puncta localize to LysoTracker® -positive compartments (B1, B2, B3, arrows). Images are single sections. Scale bar = 5 µm.

Fig. 5

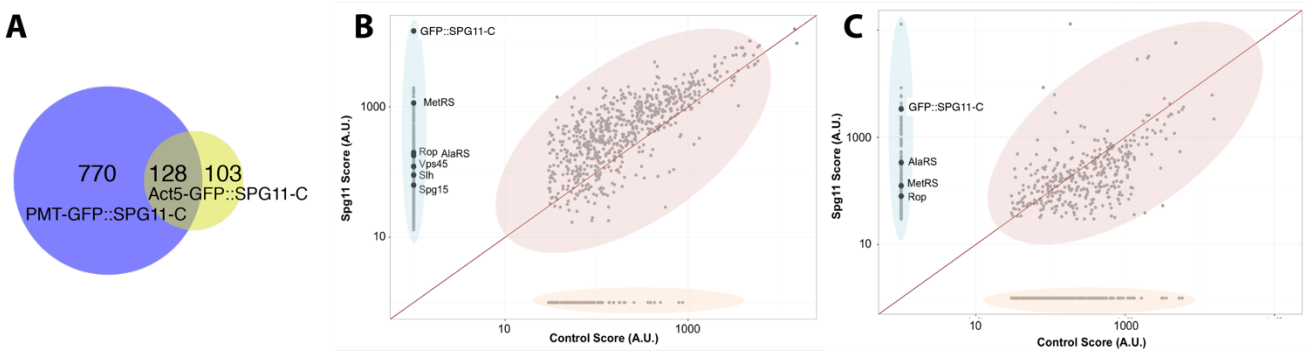

Fig. 5. Binding partners of Spg11_C identified by mass spectrometry. A. Venn diagram of Spg11_C interactors identified by mass spectrometry of PMT- GFP::Spg11-C and Act5-GFP::Spg11-C cell lines. **B,C.** Mass spectrometry output for purified GFP::Spg11-C from the *Drosophila* Mel-2 cell line expressing PMT-GFP::Spg11-C (**B**) or Act5-GFP::Spg11-C (**C**), cmopared to control cells lacking GFP::Spg11-C. Graphs plot the percentage difference between test and control. **B** has more proteins with a higher score than the equivalent protein in the negative GFP control, indicated by the majority of the protein hits residing above the equivalence line (in red). However, graph C has fewer proteins above the equivalence line. Scores of GFP::Spg11-C, Rop, Vps45, Slh, MetRS (MARS), AlaRS (AARS) and Spg15 are highlighted.

Fig. 6

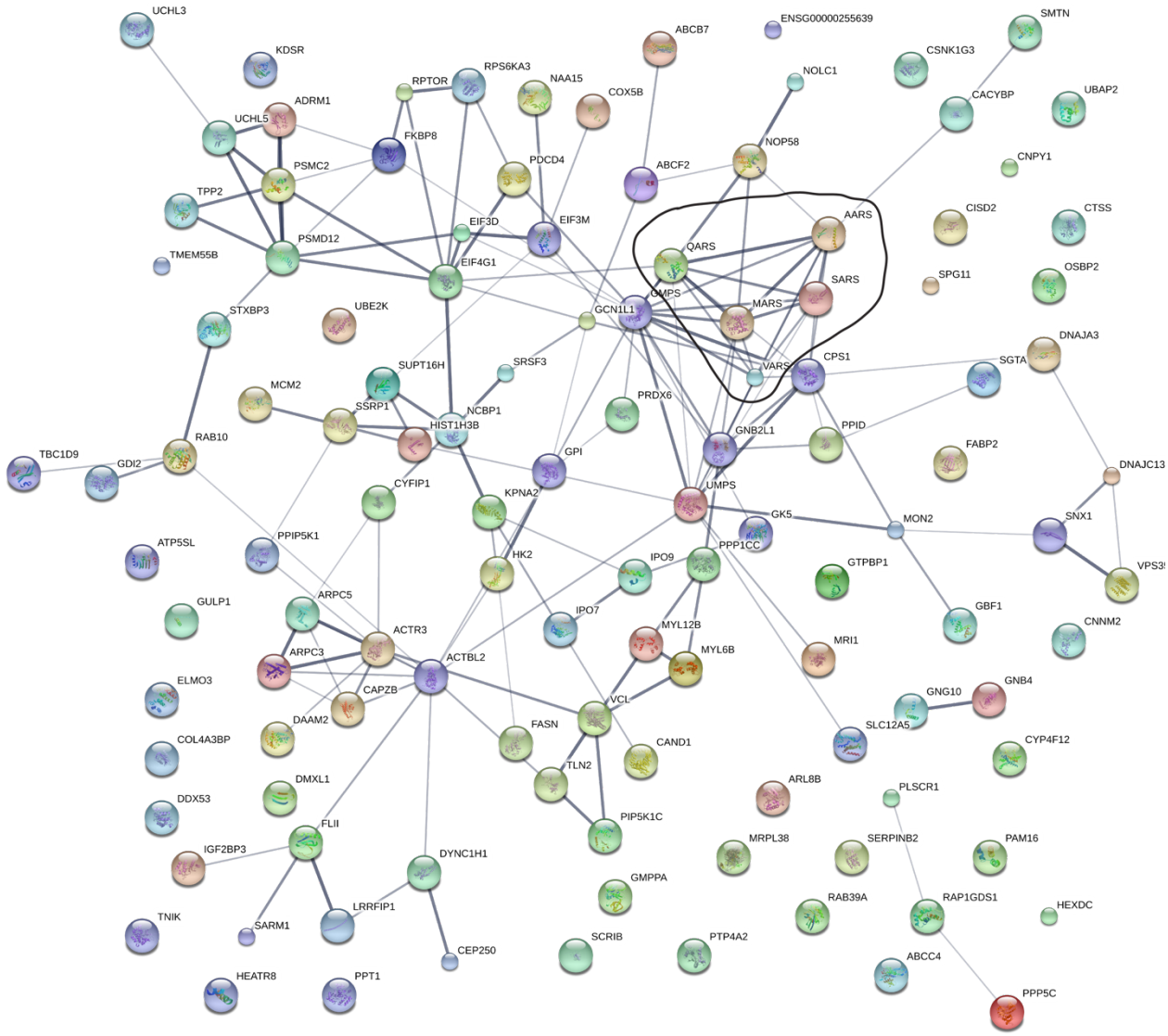

Fig. 6. Protein-protein interactome of potential Spg11 C-terminus binding partners found in both cell lines. Interactome of potential GFP::Spg11-C binding parters purified from both cell lines, generated using String (http://string-db.org). The aminoacyl-tRNA synthetases are outlined by a freehand line.

Since the Vps16_C domain of Vps16 recruits the SM proteins Vps33a to the HOPS complex (Wartosch et al., 2015), we expected to find one or more SM proteins as binding partners of the spatacsin_C domain. *Drosophila* has 5 known SM proteins (Table 5). Three of these, Rop, Vps45 and Slh were identified in the output of the $CuSO_4$-induced line (Figure 5B; Table 6). Rop was also identified in the constitutive cell line (Figure 5B; Table 6); we did not identify Vps33a (Carnation) or Vps33b as binding partners in either line.

One unexpected class of SPG11 C-terminus binding partners were aminoacyl-tRNA synthetases, which charge specific tRNAs with the correct amino acid for translation. Five of these were pulled down (Figure 6; Table 7). These included *Drosophila* homologs of the methionyl-tRNA synthetase (MARS) and alanyl-tRNA synthetase (AARS), mutations in which are causative for Charcot-Marie-Tooth (CMT) neuropathy (Gonzalez et al., 2013; McLaughlin et al., 2012; Timmerman et al., 2014), as well as serine- valine- and glutamine- tRNA synthetases (Table 7). MARS was identified with a particularly high score from the inducible line.

Discussion

Bioinformatic analyses predict functional roles of the N- and C-termini of SPG11. Our bioinformatic analyses make important functional predictions about two regions of the SPG11 protein family. First, our phylogenetic analyses show that the evolutionary presence of a conserved N-terminal region correlates strongly with the presence of the AP-5 adaptor complex, suggesting that binding to AP-5 is the only essential function of this N-terminal region. Second, the SPG11 C-terminus shows higher conservation than most other parts of SPG11, and both human and fly variants show predicted structural homology with the Vps16 C-terminus (Vps16_C, Pfam ID: PF04840) (Figure 2C). The conclusion of homology is supported by many conserved residues in a multiple sequence alignment of spatacsin_C and Vps16_C domains (Figure 3A) and tertiary structure prediction by homology (Figure 3B).

The Vps16_C domain (Pfam ID: PF04840) mediates binding to Vps33 proteins (Baker et al., 2013; Graham et al., 2013). These belong to the Sec1/Munc18 (SM) protein family (Graham et al., 2013; Misura et al., 2000) and have three domains, arranged in an arch-like structure, with an internal cavity capable of binding to SNARE proteins (Baker et al., 2013; Misura et al., 2000; Toonen and Verhage, 2003). SM proteins bind to SNARE proteins such as syntaxin and are important for membrane fusion in disparate pathways, including synapse neurotransmitter release (Harrison et al., 1994; Weimer and Richmond, 2004; Wu et al., 1998), early endosomal tracking (Nielsen et al., 2000) (Morrison et al., 2008) and Golgi-ER tracking (Laufman et al., 2009). However, their precise role is not fully understood.

Humans and flies have two Vps16 proteins: Vps16a, which binds to Vps33a in the HOPS and CORVET complexes which promote fusion of endosomes or autophagosome to lysosomes (Bröcker et al., 2012; Solinger and Spang, 2013; Urban et al., 2012), and Vps16b, which binds to Vps33b in the analogous but smaller CHEVI complex (Hunter et al., 2018; van der Beek et al., 2019). Therefore, the Spg11-C-terminal domain could potentially also bind to SM proteins; its divergence from known Vps16_C domains, and the relatively low conservation of Vps16 residues that bind to Vps33a, suggest that it is unlikely to bind to Vps33a or Vps33b, but it could potentially bind to other SM family proteins. The localization of the Spg11 C-terminus to acidic compartments (Figure 4A) could indicate a role for the Spg11-C-terminus in regulating some membrane fusion event(s) involving late endosomes, autophagosomes, autolysosomes, or lysosomes.

SPG11 C-terminus interacts with SM proteins Rop, Slh and Vps45. Mass spectrometry analysis of the SPG11 C-terminus expressed in *Drosophila* Mel-2 cells was used to identify

potential binding partners of the Spg11 C-terminus. This identified three of the five *Drosophila* SM proteins: Rop, Slh and Vps45, which were not found in the negative GFP control, tentatively indicating that the Spg11 C-terminus may possess SM protein binding ability.

Of the SM proteins identified by mass spectrometry, Rop was the highest scoring (Table 6). Rop is the homologue of yeast Sec1p (Wu et al., 1998), and is involved in synaptic vesicle exocytosis, synapse transmission and secretion (Harrison et al., 1994; Weimer and Richmond, 2004; Wu et al., 1998). Further, Sec1p stimulates *in vitro* vesicle fusion (Scott et al., 2004). Rop does not appear to bind to Vps16a or Vps16b in *Drosophila* (Pulipparacharuvil et al., 2005). Vps45 is important in the endocytic pathway (Morrison et al., 2008; Nielsen et al., 2000). In both humans and flies, Vps45 is part of a complex with Rab5 and a FYVE-containing protein, Rabenosyn-5, to mediate vesicle fusion to form early endosomes (Morrison et al., 2008; Nielsen et al., 2000). In humans *VPS45* mutations are associated with congenital neutropenia, with human *VPS45* patients lacking lysosomes (Stepensky et al., 2013). In zebrafish, the SPG15 orthologue Soue (Suf) localises with Rab5, and Rab11b, and is important for secretory vesicle maturation (Kanagaraj et al., 2014), with zebrafish *Suf* mutants showing accumulation of secretory vesicles. SPG15 also localises with Rab5 in mouse (Khundadze et al., 2013). Slh is the orthologue of yeast Sly1 (Toonen and Verhage, 2003). In mammals, Sly1 is implicated in Golgi-to-ER retrograde transport (Laufman et al., 2009; Nogueira et al., 2014). Further, Sly1 interacts with Syntaxin 18 and is important in exporting procollagen VII from the ER (Nogueira et al., 2014). SM proteins appear to have functional specificity, possibly mediated through their interactions with particular syntaxins (Toonen and Verhage, 2003).

At this stage we cannot tell whether the SM protein interactions of the Spatacsin_C domain are direct, or of functional biological significance. However, they do occur in a native Drosophila cellular environment, and they are therefore consistent with the model of a Vps16_C-like function for the Spatacsin_C domain.

The Spg11 C-terminus interacts with aminoacyl tRNA synthetases. Mass spectrometry of GFP::Spg11-C pulled down five aminoacyl-tRNA (aa-tRNA) synthetases (Figure 6A), The aa-tRNA synthetases are essential for normal protein translation, by attaching the correct amino acid onto cognate t-RNA molecules (Cusack, 1997; Datta et al., 2009; Swairjo et al., 2004; Wallen and Antonellis, 2013). However, mutations in at least two of aa-tRNA synthetases identified here, *MARS* and *AARS*, cause dominant Charcot-Marie-Tooth disease, type 2 (McLaughlin et al., 2012; Timmerman et al., 2014); furthermore, loss-of-function mutations in *SPG11* (Montecchiani et al., 2016); as well as mutations in the Spg11 binding partner, Rab7 (Gillingham et al., 2014), can cause CMTD2 (Cogli et al., 2009). Therefore, mutations affecting

SPG11, Rab7, and aa-tRNA synthetases might cause Charcot-Marie-Tooth disease by a common mechanism.

What kind of common mechanism could this be? CMT2 causality of aa-tRNA synthetases is a dominant trait that may be due to exposure of an internal surface by CMT2 mutations, and is independent of their enzymatic activity (Blocquel et al., 2017); the resulting dominant neurological CMT2 disease phenotype resemples an SPG11 recessive phenotype, suggesting that either SPG11 protein or aa-tRNA synthetases may antagonize each other. Aminoacyl tRNA synthetases have functions beyond translation, and leucyl-tRNA synthetase (LARS) is involved in amino acid sensing and autophagy regulation, by mediating mTOR activation (Bonfils et al., 2012; Han et al., 2012; Jewell et al., 2013). Further, when HeLa cells are treated with Leucine, LARS translocates to the lysosomal membrane where it acts as a GTPase-activating protein (GAP) for Rag GTPase, allowing Rag GTPase to activate mTOR (Bonfils et al., 2012; Han et al., 2012). Given that SPG11 functions on autolysosomes to regenerate lysosomes, it could interact with aa-tRNA synthetases at this location. We therefore hypothesize that CMT2 pathology could be caused by defects in autophagosomal lysosome reformation as occurs in SPG11 loss-of-function (Varga et al., 2015), and could be caused by defects in amino-acid-sensing machinery caused by gain-of-function mutations in aminoacyl-tRNA synthetases.

Conclusions. Taken together, our analyses suggest that the sole essential function of the N-terminus of SPG11 is to bind the AP-5 adaptor complex, and that its C-terminal spatacsin_C domain is a novel variant Vps_C domain, with roles in membrane trafficking. The recovery of several aminoacyl-tRNA synthetases as binding partners of this domain, suggests related mechanisms whereby mutations in human SPG11 or in aminoacyl-tRNA synthetases could give rise to Charcot-Marie-Tooth disease.

Materials and Methods

Amino acid alignments. Multiple alignments were performed using Kalign multiple alignment, with gap open penalty of 13 (http://www.ebi.ac.uk/Tools/msa/kalign/) (Lassmann and Sonnhammer, 2005), or MUSCLE multiple alignment (http://www.ebi.ac.uk/Tools/msa/muscle/) (Edgar, 2004). Pairwise alignment was performed using Matcher pairwise alignment (Zhao et al., 2013) (http://www.ebi.ac.uk/Tools/psa/emboss_matcher).

Protein function prediction. Distant structural homologs were identified using HH-pred (Söding et al., 2005) (https://toolkit.tuebingen.mpg.de/hhpred). Tertiary structure prediction by homology was performed using iTASSER tertiary structure prediction (Yang et al., 2014) (http://zhanglab.ccmb.med.umich.edu/I-TASSER/). GO term enrichment was performed using FlyMine list analysis (www.flymine.org).

Immunoprecipitation and mass spectrometry of GFP- tagged Spg11 C-terminus

We used Gateway® recombination cloning technology (Invitrogen, UK) to generate an N-terminally GFP-tagged C-terminal region of Drosophila Spg11 protein (nucleotides 3051-4094 of *Spg11* gene). The entry and destination vectors used were pDONR211 (Thermo, 12536017), Act5-Nterm GFP tag (driven by Actin5 promoter, pAGW plasmid, https://emb.carnegiescience.edu/drosophila-gateway-vector-collection) and PMT-pcBlast-Nterm GFP tag (CuSO4 Inducible promoter, Thermo V413020).

The C-terminal region of Spg11 (amino acid residues 1468-1815) was amplified using Flash High-Fidelity polymerase and extracted from electrophoresis gel using QIAquick Gel Extraction Kit according to manufacturers protocol. Primers Spg11_C_f1 (GGGGACAAGTTTGTACAAAAAAGCAGGCTTC CAC CTG TGT TTC GTG CAC GA; forward sequence annealing to codons 1468-1473, codons for HLCFVH shown as triplets) and Spg11_C_r1 (GGGGACCACTTTGTACAAGAAAGCTGGGTC CTA CGT ATC TCC TGC TGT GTG GA; complementary sequence annealing to codons 1810-1815 HTAGDT and stop, which are shown as triplets) amplified the C-terminus from codons 1468-1815; they also contained additional homology to pDONR 211 allowing homologous recombination and integration of Spg11 C-terminus. BP and LR reactions conducted according to the Gateway® recombination cloning technology manual, and transformed into DH5-alpha cells according to the manufacturers instructions (Subcloning effiency, ThermoFisher). Clones were sequenced (GATC-Biotech) using M13f and M13r primers, to ensure sequences were correct.

Transfection of *Drosophila* Mel-2 Cells. *Drosophila* Mel-2 cells (Schneider, 1972) were grown at 25°C in standard sterile cell flasks in Express SFM medium (LifeTechnologies), containing penicillin streptomycin (ThermoFisher) and L-glutamine (ThermoFisher). All cell work was carried out in a sterile fume hood. Prior to transfection, cells were grown to high confluence and seeded in 2 ml Express SFM (LifeTechnologies) in a 6-well plate, before being left for 2 hours. To transform Mel-2 cells with GFP-tagged Spg11 C-terminus, 3 µg of plasmid DNA was diluted in 100 µl ddH_2O in a microcentrifuge tube. A helper plasmid (0.5 µg) was added in parallel with Act5-Nterm GFP tag to confer Mel-2 cells with blasticidin resistance. Next, 15 µl of FuGene-HD (Promega) was applied directly to the centre of the eppendorf, and mixed thoroughly by gently pipetting up and down, before incubation for 15 minutes to allow formation of transfection complexes. Transfection mixture was added to the cells slowly, and the cell culture was subsequently incubated at 25°C for 12 hours.

Expression of GFP-tagged Spg11 C-terminus was confirmed by confocal microscopy. Mel-2 cells were seeded on sterile glass cover slips for 20 minutes, before fixing in ice cold methanol for 10 minutes. When necessary, cells were exposed to Lysotracker® for 10 minutes prior to fixation. Cells were mounted on glass slides before imaging.

Transfected Mel-2 cells were selected using blasticidin (ThermoFisher, USA) at a final concentration of 25 µg, for 5 passages. Cells were passaged when confluence approached 80%. Mel-2 cells were then expanded to $7x10^8$ in 300 ml of Express SFM medium, using large sterile conical flasks, shaken at 80 rpm at 25°C. Transgene expression was induced 24 hours prior to protein extraction by adding 500 µM CuSO4. The PMT-pcBlast-Nterm GFP tag, lacking the Spg11 C-terminus, was used as a control.

***Drosophila* Mel-2 cell immunoprecipitation.** *Drosophila* Mel-2 cells were transferred into 50 ml falcon tubles and pelleted at 5000 rpm, before resuspending cells in 8 ml of RIPA buffer (Sigma), containing protease inhibitors (Sigma). Cells lysed on ice using electronic homogeniser, 5 times, each for 30 seconds, with 30 seconds cool down time in-between. Lysed cells were centrifuged for 30 minutes at 10,000 rpm at 4°C, before collecting supernatant. For immunopreciptation, the ChromoTek GFP trap Kit A (ChromoTek, Germany) was used according to manufacturers instructions. GFP-tagged Spg11 C-terminus-bound beads were sent to for mass spectrometry analysis at the Mass Spectrometry Laboratory, Institute of Biochemistry and Biophysics, PAS. Poland.

Acknowledgements. We thank Yuu Kimata and his group for help with Drosophila cell culture and establishment of cell lines, and the Drosophila Genomics Resource Center. (supported by NIH Grant 2P40OD010949) for plasmids. This work was funded by a PhD studentship 861-792 from the UK Motor Neuron Disease Association and the Le Bouedec family to ALP, and by a grant from the Tom-Wahlig Stiftung to CJO'K.

References

Anheim, M., Lagier-Tourenne, C., Stevanin, G., Fleury, M., Durr, A., Namer, I. J., Denora, P., Brice, A., Mandel, J. L., Koenig, M., et al. (2009). SPG11 spastic paraplegia: A new cause of juvenile parkinsonism. *J. Neurol.* **256**, 104–108.

Baker, R. W., Jeffrey, P. D. and Hughson, F. M. (2013). Crystal Structures of the Sec1/Munc18 (SM) Protein Vps33, Alone and Bound to the Homotypic Fusion and Vacuolar Protein Sorting (HOPS) Subunit Vps16*. *PLoS One* **8**,.

Blocquel, D., Li, S., Wei, N., Daub, H., Sajish, M., Erfurth, M. L., Kooi, G., Zhou, J., Bai, G., Schimmel, P., et al. (2017). Alternative stable conformation capable of protein misinteraction links tRNA synthetase to peripheral neuropathy. *Nucleic Acids Res.* **45**, 8091–8104.

Bonfils, G., Jaquenoud, M., Bontron, S., Ostrowicz, C., Ungermann, C. and De Virgilio, C. (2012). Leucyl-tRNA Synthetase Controls TORC1 via the EGO Complex. *Mol. Cell* **46**, 105–110.

Boukhris, A., Stevanin, G., Feki, I., Denis, E., Elleuch, N., Miladi, M. I., Truchetto, J., Denora, P., Belal, S., Mhiri, C., et al. (2008). Hereditary spastic paraplegia with mental impairment and thin corpus callosum in Tunisia: SPG11, SPG15, and further genetic heterogeneity. *Arch. Neurol.* **65**, 393–402.

Bröcker, C., Kuhlee, A., Gatsogiannis, C., Kleine Balderhaar, H. J., Hönscher, C., Engelbrecht-Vandré, S., Ungermann, C. and Raunser, S. (2012). Molecular architecture of the multisubunit homotypic fusion and vacuole protein sorting (HOPS) tethering complex. *Proc. Natl. Acad. Sci. U. S. A.* **109**, 1991–1996.

Chang, J., Lee, S. and Blackstone, C. (2014). Spastic paraplegia proteins spastizin and spatacsin mediate autophagic lysosome reformation. *J. Clin. Invest.* **124**, 5249–5262.

Cogli, L., Piro, F. and Bucci, C. (2009). Rab7 and the CMT2B disease. In *Biochemical Society Transactions*, pp. 1027–1031.

Cusack, S. (1997). Aminoacyl-tRNA synthetases. *Curr. Opin. Struct. Biol.* **7**, 881–889.

Daoud, H., Zhou, S., Noreau, A., Sabbagh, M., Belzil, V., Dionne-Laporte, A., Tranchant, C., Dion, P. and Rouleau, G. A. (2012). Exome sequencing reveals SPG11 mutations causing juvenile ALS. *Neurobiol. Aging* **33**, 839.e5-839.e9.

Datta, D., Vaidehi, N., Zhang, D. and Goddard, W. A. (2009). Selectivity and specificity of substrate binding in methionyl-tRNA synthetase. *Protein Sci.* **13**, 2693–2705.

Edgar, R. C. (2004). MUSCLE: Multiple sequence alignment with high accuracy and high throughput. *Nucleic Acids Res.* **32**, 1792–1797.

Fridman, V. and Murphy, S. M. (2014). The spectrum of axonopathies: From CMT2 to HSP. *Neurology* **83**, 580–581.

Gillingham, A. K., Sinka, R., Torres, I. L., Lilley, K. S. and Munro, S. (2014). Toward a Comprehensive Map of the Effectors of Rab GTPases. *Dev. Cell* **31**, 358.

Gonzalez, M., McLaughlin, H., Houlden, H., Guo, M., Liu, Y. T., Hadjivassilious, M., Speziani, F., Yang, X. L., Antonellis, A., Reilly, M. M., et al. (2013). Exome sequencing identifies a significant variant in methionyl-tRNA synthetase (MARS) in a family with late-onset CMT2. *J. Neurol. Neurosurg. Psychiatry* **84**, 1247–1249.

Graham, S. C., Wartosch, L., Gray, S. R., Scourfield, E. J., Deane, J. E., Luzio, J. P. and Owen, D. J. (2013). Structural basis of Vps33A recruitment to the human HOPS complex by Vps16. *Proc. Natl. Acad. Sci. U. S. A.* **110**, 13345–13350.

Guidubaldi, A., Piano, C., Santorelli, F. M., Silvestri, G., Petracca, M., Tessa, A. and Bentivoglio, A. R. (2011). Novel mutations in SPG11 cause hereditary spastic

paraplegia associated with early-onset levodopa-responsive Parkinsonism. *Mov. Disord.* **26**, 553–556.

Han, J. M., Jeong, S. J., Park, M. C., Kim, G., Kwon, N. H., Kim, H. K., Ha, S. H., Ryu, S. H. and Kim, S. (2012). Leucyl-tRNA synthetase is an intracellular leucine sensor for the mTORC1-signaling pathway. *Cell* **149**, 410–424.

Harrison, S. D., Broadie, K., Goor, J. van de and Rubin, G. M. (1994). Mutations in the drosophila Rop gene suggest a function in general secretion and synaptic transmission. *Neuron* **13**, 555–566.

Hirst, J., Barlow, L., Francisco, G. C., Sahlender, D. A., Seaman, M. N. J., Dacks, J. B. and Robinson, M. S. (2011). The fifth adaptor protein complex. *PLoS Biol.* **9**,.

Hirst, J., Borner, G. H. H., Antrobus, R., Peden, A. A., Hodson, N. A., Sahlender, D. A. and Robinson, M. S. (2012). Distinct and overlapping roles for AP-1 and GGAs revealed by the “knocksideways” system. *Curr. Biol.* **22**, 1711–1716.

Hirst, J., Borner, G. H. H., Edgar, J., Hein, M. Y., Mann, M., Buchholz, F., Antrobus, R. and Robinson, M. S. (2013). Interaction between AP-5 and the hereditary spastic paraplegia proteins SPG11 and SPG15. *Mol. Biol. Cell* **24**, 2558–2569.

Hirst, J., Madeo, M., Smets, K., Edgar, J. R., Schols, L., Li, J., Yarrow, A., Deconinck, T., Baets, J., Van Aken, E., et al. (2016). Complicated spastic paraplegia in patients with AP5Z1 mutations (SPG48). *Neurol. Genet.* **2**,.

Hirst, J., Itzhak, D. N., Antrobus, R., Borner, G. H. H. and Robinson, M. S. (2018). Role of the AP-5 adaptor protein complex in late endosome-to-Golgi retrieval. *PLoS Biol.* **16**,.

Hunter, M. R., Hesketh, G. G., Benedyk, T. H., Gingras, A. C. and Graham, S. C. (2018). Proteomic and Biochemical Comparison of the Cellular Interaction Partners of Human VPS33A and VPS33B. *J. Mol. Biol.* **430**, 2153–2163.

Jewell, J. L., Russell, R. C. and Guan, K. L. (2013). Amino acid signalling upstream of mTOR. *Nat. Rev. Mol. Cell Biol.* **14**, 133–139.

Kanagaraj, P., Gautier-Stein, A., Riedel, D., Schomburg, C., Cerdà, J., Vollack, N. and Dosch, R. (2014). Souffle/Spastizin Controls Secretory Vesicle Maturation during Zebrafish Oogenesis. *PLoS Genet.* **10**,.

Khundadze, M., Kollmann, K., Koch, N., Biskup, C., Nietzsche, S., Zimmer, G., Hennings, J. C., Huebner, A. K., Symmank, J., Jahic, A., et al. (2013). A Hereditary Spastic Paraplegia Mouse Model Supports a Role of ZFYVE26/SPASTIZIN for the Endolysosomal System. *PLoS Genet.* **9**,.

Kim, B. Y., Krämer, H., Yamamoto, A., Kominami, E., Kohsaka, S. and Akazawa, C. (2001). Molecular Characterization of Mammalian Homologues of Class C Vps Proteins That Interact with Syntaxin-7. *J. Biol. Chem.* **276**, 29393–29402.

Lassmann, T. and Sonnhammer, E. L. L. (2005). Kalign - An accurate and fast multiple sequence alignment algorithm. *BMC Bioinformatics* **6**,.

Laufman, O., Kedan, A., Hong, W. and Lev, S. (2009). Direct interaction between the COG complex and the SM protein, Sly1, is required for Golgi SNARE pairing. *EMBO J.* **28**, 2006–2017.

Martin, E., Yanicostas, C., Rastetter, A., Naini, S. M. A., Maouedj, A., Kabashi, E., Rivaud-Péchoux, S., Brice, A., Stevanin, G. and Soussi-Yanicostas, N. (2012). Spatacsin and spastizin act in the same pathway required for proper spinal motor neuron axon outgrowth in zebrafish. *Neurobiol. Dis.* **48**, 299–308.

Mauvezin, C., Ayala, C., Braden, C. R., Kim, J. and Neufeld, T. P. (2014). Assays to monitor autophagy in Drosophila. *Methods* **68**, 134–139.

McLaughlin, H. M., Sakaguchi, R., Giblin, W., Wilson, T. E., Biesecker, L., Lupski, J. R., Talbot, K., Vance, J. M., Züchner, S., Lee, Y. C., et al. (2012). A recurrent loss-of-function alanyl-tRNA synthetase (AARS) mutation in patients with charcot-marie-tooth disease type 2N (CMT2N). *Hum. Mutat.* **33**, 244–253.

Misura, K. M. S., Scheller, R. H. and Weis, W. I. (2000). Three-dimensional structure of the neuronal-Sec1-syntaxin 1a complex. *Nature* **404**, 355–362.

Montecchiani, C., Pedace, L., Lo Giudice, T., Casella, A., Mearini, M., Gaudiello, F., Pedroso, J. L., Terracciano, C., Caltagirone, C., Massa, R., et al. (2016). ALS5/SPG11/KIAA1840 mutations cause autosomal recessive axonal Charcot-Marie-Tooth disease. *Brain* **139**, 73–85.

Morrison, H. A., Dionne, H., Rusten, T. E., Brech, A., Fisher, W. W., Pfeiffer, B. D., Celniker, S. E., Stenmark, H. and Bilder, D. (2008). RegUlation of Early Endosomal Entry by the Drosophila tumor suppressors rabenosyn and Vps45. *Mol. Biol. Cell* **19**, 4167–4176.

Murmu, R. P., Martin, E., Rastetter, A., Esteves, T., Muriel, M. P., El Hachimi, K. H., Denora, P. S., Dauphin, A., Fernandez, J. C., Duyckaerts, C., et al. (2011). Cellular distribution and subcellular localization of spatacsin and spastizin, two proteins involved in hereditary spastic paraplegia. *Mol. Cell. Neurosci.* **47**, 191–202.

Nielsen, E., Christoforidis, S., Uttenweiler-Joseph, S., Miaczynska, M., Dewitte, F., Wilm, M., Hoflack, B. and Zerial, M. (2000). Rabenosyn-5, a novel Rab5 effector, is complexed with hVPS45 and recruited to endosomes through a FYVE finger domain. *J. Cell Biol.* **151**, 601–612.

Nogueira, C., Erlmann, P., Villeneuve, J., Santos, A. J. M., Martinez-Alonso, E., Martínez-Menárguez, J. Á. and Malhotra, V. (2014). SLY1 and syntaxin 18 specify a distinct pathway for procollagen VII export from the endoplasmic reticulum. *Elife* **2014**,.

Orlacchio, A., Babalini, C., Borreca, A., Patrono, C., Massa, R., Basaran, S., Munhoz, R. P., Rogaeva, E. A., St George-Hyslop, P. H., Bernardi, G., et al. (2010). SPATACSIN mutations cause autosomal recessive juvenile amyotrophic lateral sclerosis. *Brain* **133**, 591–598.

Pensato, V., Castellotti, B., Gellera, C., Pareyson, D., Ciano, C., Nanetti, L., Salsano, E., Piscosquito, G., Sarto, E., Eoli, M., et al. (2014). Overlapping phenotypes in complex spastic paraplegias SPG11, SPG15, SPG35 and SPG48. *Brain* **137**, 1907–1920.

Pérez-Brangulí, F., Mishra, H. K., Prots, I., Havlicek, S., Kohl, Z., Saul, D., Rummel, C., Dorca-Arevalo, J., Regensburger, M., Graef, D., et al. (2014). Dysfunction of spatacsin leads to axonal pathology in SPG11-linked hereditary spastic paraplegia. *Hum. Mol. Genet.* **23**, 4859–4874.

Pulipparacharuvil, S., Akbar, M. A., Ray, S., Sevrioukov, E. A., Haberman, A. S., Rohrer, J. and Krämer, H. (2005). Drosophila Vps16A is required for trafficking to lysosomes and biogenesis of pigment granules. *J. Cell Sci.* **118**, 3663–3673.

Renvoisé, B., Chang, J., Singh, R., Yonekawa, S., FitzGibbon, E. J., Mankodi, A., Vanderver, A., Schindler, A. B., Toro, C., Gahl, W. A., et al. (2014). Lysosomal abnormalities in hereditary spastic paraplegia types SPG15 and SPG11. *Ann. Clin. Transl. Neurol.* **1**, 379–389.

Rohrer, J., Schweizer, A., Russell, D. and Kornfeld, S. (1996). The targeting of lamp1 to lysosomes is dependent on the spacing of its cytoplasmic tail tyrosine sorting motif relative to the membrane. *J. Cell Biol.* **132**, 565–576.

Schneider, I. (1972). Cell lines derived from late embryonic stages of Drosophila melanogaster. *J. Embryol. Exp. Morphol.* **27**, 353–365.

Schröder, B., Wrocklage, C., Pan, C., Jäger, R., Kösters, B., Schäfer, H., Elsässer, H. P., Mann, M. and Hasilik, A. (2007). Integral and associated lysosomal membrane proteins. *Traffic* **8**, 1676–1686.

Scott, R. C., Schuldiner, O. and Neufeld, T. P. (2004). Role and regulation of starvation-induced autophagy in the Drosophila fat body. *Dev. Cell* **7**, 167–178.

Słabicki, M., Theis, M., Krastev, D. B., Samsonov, S., Mundwiller, E., Junqueira, M., Paszkowski-Rogacz, M., Teyra, J., Heninger, A. K., Poser, I., et al. (2010). A genome-scale DNA repair RNAi screen identifies SPG48 as a novel gene associated with hereditary spastic paraplegia. *PLoS Biol.* **8**,.

Söding, J., Biegert, A. and Lupas, A. N. (2005). The HHpred interactive server for protein homology detection and structure prediction. *Nucleic Acids Res.* **33**,.

Solinger, J. A. and Spang, A. (2013). Tethering complexes in the endocytic pathway: CORVET and HOPS. *FEBS J.* **280**, 2743–2757.

Stepensky, P., Saada, A., Cowan, M., Tabib, A., Fischer, U., Berkun, Y., Saleh, H., Simanovsky, N., Kogot-Levin, A., Weintraub, M., et al. (2013). The Thr224Asn mutation in the VPS45 gene is associated with the congenital neutropenia and primary myelofibrosis of infancy. *Blood* **121**, 5078–5087.

Stevanin, G., Santorelli, F. M., Azzedine, H., Coutinho, P., Chomilier, J., Denora, P. S., Martin, E., Ouvrard-Hernandez, A. M., Tessa, A., Bouslam, N., et al. (2007). Mutations in SPG11, encoding spatacsin, are a major cause of spastic paraplegia with thin corpus callosum. *Nat. Genet.* **39**, 366–372.

Swairjo, M. A., Otero, F. J., Yang, X. L., Lovato, M. A., Skene, R. J., McRee, D. E., De Pouplana, L. R. and Schimmel, P. (2004). Alanyl-tRNA synthetase crystal structure and design for acceptor-stem recognition. *Mol. Cell* **13**, 829–841.

Szymanski, C. J., Humphries IV, W. H. and Payne, C. K. (2011). Single particle tracking as a method to resolve differences in highly colocalized proteins. *Analyst* **136**, 3527–3533.

Timmerman, V., Strickland, A. V. and Züchner, S. (2014). Genetics of Charcot-Marie-Tooth (CMT) disease within the frame of the human genome project success. *Genes (Basel).* **5**, 13–32.

Toonen, R. F. G. and Verhage, M. (2003). Vesicle trafficking: Pleasure and pain from SM genes. *Trends Cell Biol.* **13**, 177–186.

Urban, D., Li, N., Christensen, H., Pluthero, F. G., Chen, S. Z., Puhacz, M., Garg, P. M., Lanka, K. K., Cummings, J. J., Kramer, H., et al. (2012). The VPS33B-binding protein VPS16B is required in megakaryocyte and platelet α-granule biogenesis. *Blood* **120**, 5032–5040.

van der Beek, J., Jonker, C., van der Welle, R., Liv, N. and Klumperman, J. (2019). CORVET, CHEVI and HOPS – Multisubunit tethers of the endo-lysosomal system in health and disease. *J. Cell Sci.* **132**,.

Vantaggiato, C., Crimella, C., Airoldi, G., Polishchuk, R., Bonato, S., Brighina, E., Scarlato, M., Musumeci, O., Toscano, A., Martinuzzi, A., et al. (2013). Defective autophagy in spastizin mutated patients with hereditary spastic paraparesis type 15. *Brain* **136**, 3119–3139.

Varga, R. E., Khundadze, M., Damme, M., Nietzsche, S., Hoffmann, B., Stauber, T., Koch, N., Hennings, J. C., Franzka, P., Huebner, A. K., et al. (2015). In Vivo Evidence for Lysosome Depletion and Impaired Autophagic Clearance in Hereditary Spastic Paraplegia Type SPG11. *PLoS Genet.* **11**,.

Wallen, R. C. and Antonellis, A. (2013). To charge or not to charge: Mechanistic insights into neuropathy-associated tRNA synthetase mutations. *Curr. Opin. Genet. Dev.* **23**,

302–309.

Wartosch, L., Günesdogan, U., Graham, S. C. and Luzio, J. P. (2015). Recruitment of VPS33A to HOPS by VPS16 Is Required for Lysosome Fusion with Endosomes and Autophagosomes. *Traffic* **16**, 727–742.

Weimer, R. M. and Richmond, J. E. (2004). Synaptic Vesicle Docking: A Putative Role for the Munc18{plus 45 degree rule}Sec1 Protein Family. *Curr. Top. Dev. Biol.* **65**, 83–113.

Wu, M. N., Littleton, J. T., Bhat, M. A., Prokop, A. and Bellen, H. J. (1998). ROP, the Drosophila Sec1 homolog, interacts with syntaxin and regulates neurotransmitter release in a dosage-dependent manner. *EMBO J.* **17**, 127–139.

Yang, J., Yan, R., Roy, A., Xu, D., Poisson, J. and Zhang, Y. (2014). The I-TASSER suite: Protein structure and function prediction. *Nat. Methods* **12**, 7–8.

Yu, L., McPhee, C. K., Zheng, L., Mardones, G. A., Rong, Y., Peng, J., Mi, N., Zhao, Y., Liu, Z., Wan, F., et al. (2010). Termination of autophagy and reformation of lysosomes regulated by mTOR. *Nature* **465**, 942–946.

Zhao, W., Zhu, Q. Y., Zhang, J. T., Liu, H., Wang, L. J., Chen, Z. Q., Guan, L. P., Huang, X. S., Yang, L. and Yu, S. Y. (2013). Exome sequencing identifies novel compound heterozygous mutations in SPG11 that cause autosomal recessive hereditary spastic paraplegia. *J. Neurol. Sci.* **335**, 112–117.

Table 1. Top 100 unique hits found in mass spectrometry output from GFP::Spg11-C purification from PMT-GFP::Spg11-C. Biological process and human ortholog (Human Ortho) data are from Flybase (www.flybase.org). Some of the hits discussed in the text are in bold.

Gene	Protein	CDS	Score	Matches	Sequences	Biological Process	Cellular Component	Human Ortho
CG13531	**CG13531**	**PB**	**14611**	**290**	**17**	**axon extension**	**axon**	**SPG11**
CG11700	CG11700	PB	1876	82	5	protein ubiquitination	microtubule associated complex	RPS27A
deltaCOP	**CG14813**	**PA**	**1813**	**41**	**13**	**retrograde vesicle-mediated transport, Golgi to ER**	**COPI vesicle coat**	**ARCN1**
CG30109	CG30109	PB	1771	27	3	biological_process	cellular_component	TRIAP1
Cisd2	**CG1458**	**PA**	**1630**	**28**	**3**	**biological_process**	**intracellular membrane-bounded organelle**	**CISD2**
Prx2540-2	CG11765	PA	1604	51	11	cell redox homeostasis	cytosol	PRDX6
Prx2540-1	CG12405	PA	1430	47	10	hydrogen peroxide catabolic process	cytosol	PRDX6
CG12896	CG12896	PA	1193	40	9	mesoderm development	cytoplasm	PRDX6
Dgp-1	CG5729	PA	1192	25	10	biological_process	cellular_component	GTPBP1
Rep	CG8432	PA	1192	25	8	neurotransmitter secretion	Rab-protein geranylgeranyltransferase complex	CHM
MetRS	**CG15100**	**PA**	**1147**	**26**	**14**	**methionyl-tRNA aminoacylation**	**microtubule associated complex**	**MARS**
Aldh-III	CG11140	PE	1087	25	10	oxidation-reduction process	lipid particle	GK5
Prosalpha 2	CG5266	PA	1053	21	5	proteasome-mediated ubiquitin-dependent protein catabolic process	proteasome core complex	PSMA7
mys	CG1560	PA	969	23	7	central nervous system development	focal adhesion	ITGB8
mys	CG1560	PB	916	21	6	central nervous system development	focal adhesion	ITGB8
su(r)	CG2194	PC	913	18	11	'de novo' pyrimidine nucleobase biosynthetic process	cytoplasm	DPYD
eEF1delta	CG4912	PA	892	16	5	translational elongation	eukaryotic translation elongation factor 1 complex	EEF1D
Msp300	CG42768	PG	797	18	15	mesoderm development	actin cytoskeleton	SYNE2
Msp300	CG42768	PD	796	17	14	mesoderm development	actin cytoskeleton	SYNE2
Hsp27	CG4466	PA	794	14	3	determination of adult lifespan	microtubule associated complex	HSPB6
eIF4G	CG10811	PA	741	19	13	translational initiation	cytosol	EIF4G1
smid	CG8571	PA	710	11	5	neurogenesis	-	NVL
Usp14	CG5384	PA	700	10	5	ubiquitin-dependent protein catabolic process	microtubule associated complex	USP14
Prosalpha 3	CG9327	PA	682	16	5	ubiquitin-dependent protein catabolic process	cytoplasm	PSMA4
CG8005	CG8005	PA	675	16	6	peptidyl-lysine modification to peptidyl-hypusine	-	DHPS
r	CG18572	PA	652	17	12	'de novo' pyrimidine nucleobase biosynthetic process	cytoplasm	CPS1
CG17514	CG17514	PA	651	18	13	regulation of translation	-	GCN1
Tango7	**CG8309**	**PA**	**632**	**15**	**7**	**Golgi organization**	**Golgi apparatus**	**EIF3M**
Rpn5	CG1100	PA	627	19	9	proteasome-mediated ubiquitin-dependent protein catabolic process	proteasome regulatory particle	PSMD12
nop5	CG10206	PA	605	12	7	rRNA processing	nucleolus	NOP58
Ts	CG3181	PA	591	7	3	deoxyribonucleotide biosynthetic process	-	TYMS
Cp1	CG6692	PA	590	15	4	protein catabolic process	lysosome	CTSS
Mrp4	CG14709	PB	588	13	9	drug transmembrane transport	ATP-binding cassette (ABC) transporter complex	ABCC4
Dhc64C	**CG7507**	**PA**	**582**	**14**	**11**	**cellularization**	**cytoplasm**	**DYNC1H1**
rhea	CG6831	PB	526	13	9	cytoskeletal anchoring at plasma membrane	focal adhesion	TLN2

CG7945	CG7945	PA	524	9	5	protein folding	-	BAG2
poe	CG14472	PA	519	15	12	spermatid development	P granule	UBR4
CG7945	CG7945	PB	510	8	4	protein folding	-	BAG2
msk	CG7935	PA	475	10	6	protein import into nucleus	cytoplasm	IPO7
CG10289	CG10289	PA	474	9	7	-	-	
ade5	CG3989	PA	461	11	6	inter-male aggressive behavior	cytoplasm	PAICS
hts	CG43443	PA	452	8	5	axon guidance	lipid particle	
Rpt6R	CG2241	PA	440	14	5	neurogenesis	microtubule associated complex	PSMC2
Prosalpha 4	CG3422	PA	434	10	4	cellular response to DNA damage stimulus	microtubule associated complex	PSMA7
Rpn7	CG5378	PA	420	10	4	proteolysis	proteasome regulatory particle, lid subcomplex	PSMD6
pic	CG7769	PA	418	16	6	positive regulation of protein catabolic process	nucleus	DDB1
Cand1	CG5366	PA	415	6	3	regulation of protein stability	-	CAND1
Prosalpha 6	CG4904	PB	409	12	6	proteasome-mediated ubiquitin-dependent protein catabolic process	cytoplasm	PSMA1
FKBP59	CG4535	PA	402	12	6	peripheral nervous system development	inaD signaling complex	FKBP5
kcc	CG5594	PE	391	8	5	transport	integral component of membrane	SLC12A5
eIF-2beta	CG4153	PA	388	7	2	translational initiation	cytosol	EIF2S2
Uch-L5	CG3431	PA	382	12	5	protein deubiquitination	proteasome regulatory particle	UCHL5
Rab35	**CG9575**	**PA**	**379**	**12**	**3**	**mitotic cytokinesis**	**lipid particle**	**RAB8B**
Int6	CG9677	PA	376	9	5	translational initiation	eukaryotic translation initiation factor 3 complex	EIF3E
CG31918	CG31918	PA	375	10	6	proteolysis	-	PHEX
Mfe2	CG3415	PA	368	7	4	fatty acid beta-oxidation using acyl-CoA oxidase	peroxisome	HSD17B4
ND-75	CG2286	PA	362	10	8	cellular respiration	mitochondrial respiratory chain complex I	NDUFS1
Pect	CG5547	PB	362	12	7	ethanolamine-containing compound metabolic process	-	PCYT2
MAPk-Ak2	CG3086	PB	360	9	4	protein phosphorylation	cytoplasm	MAPKAPK5
Prosalpha 7	CG1519	PA	358	11	6	cellular response to DNA damage stimulus	microtubule associated complex	PSMA3
l(1)G0193	CG2206	PA	355	7	6	biological_process	cellular_component	
Ugt	CG6850	PA	348	4	4	protein glycosylation	cytoplasm	UGGT1
Rab4	**CG4921**	**PB**	**347**	**8**	**2**	**ovarian follicle cell-cell adhesion**	**synapse**	**RAB4B**
MtnA	CG9470	PA	346	10	2	response to metal ion	cellular_component	
CG10527	CG10527	PA	344	11	4	-	cytoplasm	
grsm	CG7340	PB	344	7	4	proteolysis	cytoplasm	NPEPL1
kcc	CG5594	PC	343	6	4	transport	integral component of membrane	SLC12A5
UQCR-14	CG3560	PA	342	10	5	mitochondrial electron transport, ubiquinol to cytochrome c	mitochondrial respiratory chain complex III	UQCRB
SerRS	**CG17259**	**PA**	**341**	**6**	**4**	**seryl-tRNA aminoacylation**	**cytoplasm**	**SARS**
rump	CG9373	PA	340	9	3	anterior/posterior axis specification, embryo	nuclear chromatin	MYEF2
smt3	CG4494	PA	337	6	2	phagocytosis	nucleus	SUMO2
PpD3	CG8402	PB	330	5	3	protein dephosphorylation	nucleus	PPP5C
rush	**CG14782**	**PA**	**329**	**10**	**4**	**neuron projection morphogenesis**	**early endosome**	**PLEKHF1**
CG9674	CG9674	PA	323	8	6	oxidation-reduction process	-	FDXR
CG1598	CG1598	PA	320	6	3	-	-	ASNA1
CG32576	**CG32576**	**PA**	**320**	**3**	**1**	**vesicle-mediated transport**	**cellular_component**	**GOLT1B**
Cyp9c1	CG3616	PA	319	5	4	oxidation-reduction process	membrane	CYP4F12
Prosalpha 5	CG10938	PA	317	11	5	proteasome-mediated ubiquitin-dependent protein catabolic process	proteasome core complex, alpha-subunit complex	PSMA5
Cklalpha	CG2028	PB	315	6	3	DNA repair	cytoplasm	CSNK1A1L
Mi-2	CG8103	PA	307	5	3	negative regulation of cohesin loading	nucleus	CHD3

CG40045	CG40045	PA	305	8	2	protein polyubiquitination	cellular_component	CDC34
Rpn12	CG4157	PA	300	5	3	neurogenesis	proteasome regulatory particle	PSMD8
Sgt	CG5094	PA	297	9	5	neuromuscular synaptic transmission	cellular_component	SGTA
COX5B	CG11015	PA	296	8	2	mitochondrial electron transport, cytochrome c to oxygen	mitochondrion	COX5B
kcc	CG5594	PA	294	6	3	transport	integral component of membrane	SLC12A5
Prx3	CG5826	PA	294	9	5	cell redox homeostasis	mitochondrion	PRDX2
emb	CG13387	PA	292	8	5	protein export from nucleus	nuclear pore	XPO1
CG9391	CG9391	PA	291	5	3	dephosphorylation	cytoplasm	IMPA2
Sec22	**CG7359**	**PA**	**290**	**5**	**2**	**vesicle-mediated transport**	**transport vesicle**	**SEC22B**
sqh	**CG3595**	**PA**	**283**	**6**	**3**	**ovarian follicle cell development**	**unconventional myosin complex**	**MYL12B**
LKRSDH	CG7144	PA	281	6	5	regulation of histone methylation	-	AASS
Exo84	CG6095	PA	279	4	3	meiotic spindle organization	exocyst	EXOC8
FK506-bp1	CG6226	PA	278	6	2	protein folding	nucleus	PPID
Prosbeta1	CG8392	PA	278	8	3	cellular response to DNA damage stimulus	proteasome core complex	PSMB6
poly	CG9829	PA	277	3	2	oocyte microtubule cytoskeleton polarization	cellular_component	
Arpc5	CG9881	PA	270	8	5	cell morphogenesis	lamellipodium	ARPC5
CG1640	CG1640	PB	269	6	5	biosynthetic process	mitochondrion	GPT2
Rab35	**CG9575**	**PC**	**268**	**8**	**2**	**mitotic cytokinesis**	**lipid particle**	**RAB8B**
Ppt1	**CG12108**	**PA**	**267**	**9**	**4**	**macromolecule depalmitoylation**	**lysosome**	**PPT1**

Table 2. Top 100 unique hits found in mass spectrometry output from GFP::Spg11-C purification from Act-Spg11- C::GFP. Biological process and human ortholog (Human Ortho) data from Flybase (www.flybase.org). Some of the hits discussed in the text are in bold.

Gene	Protein	CDS	Score	Matches	Sequences	Biological Process	Cellular Component	Human Ortho
Mlc-c	**CG3201**	**PA**	**8379**	**178**	**11**	**actin filament-based movement**	**myosin complex**	**MYL6B**
sqh	**CG3595**	**PA**	**5723**	**117**	**8**	**ovarian follicle cell development**	**unconventional myosin complex**	**MYL12B**
Actn	CG4376	PA	4354	115	28	actin filament bundle assembly	focal adhesion	ACTN4
Gel	CG1106	PA	3844	103	23	phagocytosis	actin filament	AVIL
CG13531	**CG13531**	**PB**	**3373**	**81**	**13**	**axon extension**	**axon**	**SPG11**
Swip-1	CG10641	PA	2215	43	9	mesoderm development	muscle tendon junction	EFHD1
cpb	CG17158	PA	1892	39	10	microtubule-based movement	dynactin complex	CAPZB
cpa	CG10540	PA	1701	44	9	actin filament organization	dynactin complex	CAPZA1
Arp3	CG7558	PA	1452	35	11	actin cytoskeleton organization	actin filament	ACTR3
didum	CG2146	PA	1215	28	13	anterior/posterior axis specification, embryo	myosin complex	MYO5B
Arpc2	CG10954	PA	1171	43	6	lateral inhibition	Arp2/3 protein complex	ARPC2
didum	CG2146	PB	931	23	11	anterior/posterior axis specification, embryo	myosin complex	MYO5B
CG15099	CG15099	PA	882	15	3			DOPEY2
Arp53D	CG5409	PB	829	40	2	cytoskeleton organization	actin filament	ACTBL2
Cisd2	**CG1458**	**PA**	**801**	**17**	**3**		**intracellular membrane-bounded organelle**	**CISD2**
msk	CG7935	PA	775	12	5	protein import into nucleus	cytoplasm	IPO7
Arpc1	CG8978	PB	772	22	9	actin filament polymerization	Arp2/3 protein complex	ARPC1B
Arpc3A	CG4560	PC	690	13	4	Arp2/3 complex-mediated actin nucleation	Arp2/3 protein complex	ARPC3
CG6707	**CG6707**	**PA**	**540**	**19**	**4**	**phosphatidylinositol dephosphorylation**	**lysosomal membrane**	**TMEM55B**
Hmt-1	CG4225	PA	534	8	2	heme transport	ATP-binding cassette (ABC) transporter complex	ABCB7
ck	CG7595	PA	507	11	6	sensory perception of sound	unconventional myosin complex	MYO7B
CG32521	CG32521	PA	446	7	2	-	-	
tmod	CG1539	PA	442	11	5	cytoskeleton organization	fusome	
mon2	CG8683	PB	391	10	6	pole plasm protein localization	endosome	MON2
eIF4G	CG10811	PA	384	6	3	translational initiation	cytosol	EIF4G1
CG4042	CG4042	PA	380	24	1	-	-	ATP5SL
Gie	**CG7891**	**PA**	**380**	**6**	**2**	**sister chromatid segregation**	**lysosome**	**ARL8B**
CG8578	CG8578	PA	348	6	4	adult somatic muscle development	-	LRRFIP1
CG32521	CG32521	PG	338	4	1	-	-	
AlaRS	**CG13391**	**PB**	**338**	**5**	**2**	**alanyl-tRNA aminoacylation**	**cytoplasm**	**AARS**
ValRS	**CG4062**	**PB**	**331**	**5**	**3**	**valyl-tRNA aminoacylation**	**cytoplasm**	**VARS**
CG7806	CG7806	PA	313	8	4	transmembrane transport	integral component of membrane	ABCC4
Cp1	CG6692	PA	303	7	2	protein catabolic process	lysosome	CTSS
Aldh-III	CG11140	PE	285	6	3	oxidation-reduction process	lipid particle	GK5
FASN1	CG3523	PA	285	5	5	triglyceride biosynthetic process	lipid particle	FASN
Arpc5	CG9881	PA	278	7	1	cell morphogenesis	lamellipodium	ARPC5
CG4552	CG4552	PA	276	4	2	border follicle cell migration	-	TBC1D23
jar	CG5695	PB	271	8	4	membrane organization	unconventional myosin complex	MYO6
Pp1-87B	CG5650	PA	262	4	2	protein dephosphorylation	protein phosphatase type 1 complex	PPP1CC
CG31729	CG31729	PA	238	5	2	phospholipid translocation	integral component of membrane	ATP9B
pav	**CG1258**	**PA**	**228**	**5**	**4**	**neurogenesis**	**kinesin complex**	**KIF23**

CG17272	CG17272	PA	226	3	2	-	-	
r	CG18572	PA	225	6	2	'de novo' pyrimidine nucleobase biosynthetic process	cytoplasm	CPS1
Tango7	**CG8309**	**PA**	**220**	**3**	**1**	**Golgi organization**	**Golgi apparatus**	**EIF3M**
RhoGDI	CG7823	PA	211	7	2	-	cytoplasm	ARHGDIA
Cand1	CG5366	PA	207	2	2	regulation of protein stability	-	CAND1
PRL-1	CG4993	PA	206	3	2	protein dephosphorylation	cytoplasm	PTP4A2
Rack1	CG7111	PA	206	7	3	oviposition	cytoplasm	GNB2L1
Snx1	**CG2774**	**PA**	**205**	**5**	**1**	**intracellular protein transport**	**retromer, tubulation complex**	**SNX1**
CG11334	CG11334	PA	202	5	1	translation	eukaryotic translation initiation factor 2B complex	MRI1
Rab39	**CG12156**	**PA**	**198**	**7**	**2**	**Rab protein signal transduction**	**Golgi apparatus**	**RAB39A**
Arp2	CG9901	PA	194	6	3	cytoskeleton organization	actin filament	ACTR2
RabX4	**CG31118**	**PA**	**179**	**6**	**1**	**Rab protein signal transduction**	**synapse**	**RAB10**
Arpc4	CG5972	PA	177	6	4	cell projection assembly	Arp2/3 protein complex	ARPC4
Iva	**CG6450**	**PC**	**177**	**4**	**2**	**cellularization**	**Golgi apparatus**	**CEP250**
FK506-bp1	CG6226	PA	176	7	4	protein folding	nucleus	PPID
rhea	CG6831	PB	172	2	2	cytoskeletal anchoring at plasma membrane	focal adhesion	TLN2
row	CG8092	PA	170	3	1	regulation of transcription, DNA-templated	protein complex	
Pgi	CG8251	PA	169	2	1	gluconeogenesis	lipid particle	GPI
Osbp	**CG6708**	**PA**	**167**	**2**	**2**	**sperm individualization**	**endoplasmic reticulum**	**OSBP2**
uex	CG42595	PE	162	5	2	cellular ion homeostasis	cellular_component	CNNM2
Hex-A	CG3001	PA	159	2	1	carbohydrate phosphorylation	-	HK2
msn	CG16973	PA	158	9	2	photoreceptor cell morphogenesis	cell cortex	TNIK
vimar	CG3572	PB	154	4	1	tricarboxylic acid cycle	plasma membrane	RAP1GDS1
Rack1	CG7111	PB	151	4	2	oviposition	cytoplasm	GNB2L1
Glt	CG9280	PA	150	1	1	synaptic target inhibition	basement membrane	
Rpn13	CG13349	PA	146	3	2	lateral inhibition	proteasome regulatory particle	ADRM1
CG9281	CG9281	PB	144	4	1	-	ATP-binding cassette (ABC) transporter complex	ABCF2
alien	CG9556	PA	141	1	1	protein stabilization	COP9 signalosome	
Dhc64C	**CG7507**	**PA**	**138**	**4**	**4**	**cellularization**	**cytoplasm**	**DYNC1H1**
CG7878	CG7878	PA	136	4	2	-	-	DDX53
Kap-alpha3	CG9423	PA	135	1	1	protein import into nucleus	nuclear pore	KPNA2
SerRS	**CG17259**	**PA**	**135**	**2**	**1**	**seryl-tRNA aminoacylation**	**cytoplasm**	**SARS**
Rme-8	**CG8014**	**PA**	**133**	**4**	**3**	**endocytosis**	**microtubule associated complex**	**DNAJC13**
Pp1-Y2	CG40448	PB	131	2	1	protein dephosphorylation	nucleus	PPP1CC
Gbeta13F	CG10545	PB	129	2	1	actin filament organization	heterotrimeric G-protein complex	GNB4
CG5482	CG5482	PA	129	2	1	protein folding	endomembrane system	FKBP8
Imp	CG1691	PC	126	2	1	nervous system development	precatalytic spliceosome	IGF2BP3
Stam	CG6521	PA	125	3	1	JAK-STAT cascade	ESCRT-0 complex	STAM2
MetRS	**CG15100**	**PA**	**125**	**1**	**1**	**methionyl-tRNA aminoacylation**	**microtubule associated complex**	**MARS**
CG12065	CG12065	PA	124	2	1	lateral inhibition	-	
SPARC	CG6378	PA	123	2	1	cell adhesion	basement membrane	SPARCL1
Gdi	**CG4422**	**PA**	**119**	**2**	**2**	**neurotransmitter secretion**	**synaptic vesicle**	**GDI2**
Mrp4	CG14709	PB	118	1	1	drug transmembrane transport	ATP-binding cassette (ABC) transporter complex	ABCC4
CG9044	CG9044	PB	118	1	1	protein localization	cytoplasm	STK11IP
msn	CG16973	PB	117	8	1	photoreceptor cell morphogenesis	cell cortex	TNIK
Flo2	CG32593	PF	117	2	2	cell adhesion	flotillin complex	FLOT2

CG10425	CG10425	PA	116	1	1	-	-	KDSR
raptor	**CG4320**	**PB**	**114**	**3**	**2**	**positive regulation of protein phosphorylation**	**TORC1 complex**	**RPTOR**
shot	CG18076	PA	114	1	1	muscle attachment	fusome	SMTN
Flo2	CG32593	PC	107	1	1	cell adhesion	flotillin complex	FLOT2
Cyp9c1	CG3616	PA	107	1	1	oxidation-reduction process	membrane	CYP4F12
Klp61F	**CG9191**	**PA**	**105**	**2**	**2**	**neurogenesis**	**cytoplasm**	**KIF11**
PpD3	CG8402	PB	103	3	1	protein dephosphorylation	nucleus	PPP5C
blp	CG5268	PA	101	1	1	embryonic development via the syncytial blastoderm	cellular_component	PAM16
CG8336	CG8336	PB	99	6	1	protein folding	-	PPID
CG3587	CG3587	PA	98	2	1	-	-	KTI12
CG30122	CG30122	PB	98	1	1	mRNA splicing, via spliceosome	precatalytic spliceosome	
Vps35	**CG5625**	**PA**	**98**	**1**	**1**	**vesicle-mediated transport**	**endosome**	**VPS35**

Table 3. Protein hits identified from GFP::Spg11-C purification from both Act5-GFP::Spg11-C and PMT-GFP::Spg11-C. Proteins are ranked by highest score present in either of the two lines. Proteins mentioned in the text are highlighted. Human orthologue (Human Orth) data are from Flybase (www.flybase.org). Some of the hits discussed in the text are in bold.

#	Protein	Gene	Human Orth	#	Protein	Gene	Human Orth	#	Protein	Gene	Human Orth
1	**CG13531**	***CG13531***	**SPG11**	**51**	**CG15811**	***Rop***	**STXBP3**	**101**	CG1828	*dre4*	SUPT16H
2	CG5409	*Arp53D*	ACTBL2	**52**	CG13849	*Nop56*	NOP58	**102**	CG7207	*cert*	COL4A3BP
3	CG2241	*Rpt6R*	PSMC2	**53**	CG10990	*Pdcd4*	PDCD4	**103**	CG6020	*ND-39*	ENS G00000255639
4	CG7878	*CG7878*	DDX53	**54**	CG5650	*Pp1-87B*	PPP1CC	**104**	CG5336	*Ced-12*	ELMO3
5	CG1458	*Cisd2*	CISD2	**55**	CG3523	*FASN1*	FASN	**105**	CG1484	*flil*	FLII
6	CG11765	*Prx2540-2*	PRDX6	**56**	CG5504	*l(2)tid*	DNAJA3	**106**	CG4993	*PRL-1*	PTP4A2
7	**CG12156**	***Rab39***	**RAB39A**	**57**	CG3991	*TppII*	TPP2	**107**	CG4042	*CG4042*	ATP5SL
8	**CG31118**	***RabX4***	**RAB10**	**58**	CG12400	*ND-B14.5B*		**108**	CG43398	*scrib*	SCRIB
9	CG5729	*Dgp-1*	GTPBP1	**59**	CG11804	*ced-6*	GULP1	**109**	**CG2774**	***Snx1***	**SNX1**
10	**CG15100**	***MetRS***	**MARS**	**60**	**CG3201**	***Mlc-c***	**MYL6B**	**110**	CG6963	*gish*	CSNK1G3
11	CG11140	*Aldh-III*	GK5	**61**	CG10539	*S6k*	RPS6KA3	**111**	CG12202	*NAA15-16*	NAA15
12	CG15871	*mRpL38*	MRPL38	**62**	**CG5625**	***Vps35***	**VPS35**	**112**	CG5482	*CG5482*	FKBP8
13	CG10811	*eIF4G*	EIF4G1	**63**	CG4931	*Sra-1*	CYFIP1	**113**	**CG6708**	***Osbp***	**OSBP2**
14	CG18572	*r*	CPS1	**64**	CG1987	*Rbp1-like*	SRSF3	**114**	CG17158	*cpb*	CAPZB
15	CG17514	*CG17514*	GCN1	**65**	CG18076	*shot*	SMTN	**115**	CG9186	*CG9186*	LDAH
16	**CG8309**	***Tango7***	**EIF3M**	**66**	CG32056	*scramb1*	PLSCR1	**116**	**CG6450**	***Iva***	**CEP250**
17	CG1100	*Rpn5*	PSMD12	**67**	CG30122	*CG30122*		**117**	CG8578	*CG8578*	LRRFIP1
18	CG10206	*nop5*	NOP58	**68**	CG7558	*Arp3*	ACTR3	**118**	CG7421	*Nopp140*	NOLC1
19	CG6692	*Cp1*	CTSS	**69**	CG7324	*CG7324*	TBC1D9	**119**	CG8207	*CG8207*	GMPPA
20	CG14709	*Mrp4*	ABCC4	**70**	**CG4062**	***ValRS***	**VARS**	**120**	CG30159	*CG30159*	
21	**CG7507**	***Dhc64C***	**DYNC1H1**	**71**	CG7111	*Rack1*	GNB2L1	**121**	CG7985	*CG7985*	HEXDC
22	CG6831	*rhea*	TLN2	**72**	**CG10506**	***GlnRS***	**QARS**	**122**	CG43947	*PsGEF*	
23	CG7935	*msk*	IPO7	**73**	CG8261	*Ggamma1*	GNG10	**123**	CG7035	*Cbp80*	NCBP1
24	CG43443	*hts*		**74**	CG3585	*Rbcn-3A*	DMXL1	**124**	CG5268	*blp*	PAM16
25	CG5366	*Cand1*	CAND1	**75**	CG32138	*Frl*	DAAM2	**125**	CG8989	*His3.3B*	HIST1H3B
26	CG5594	*kcc*	SLC12A5	**76**	CG4422	*Gdi*	GDI2	**126**	CG7538	*Mcm2*	MCM2
27	CG3431	*Uch-L5*	UCHL5	**77**	CG3299	*Vinc*	VCL	**127**	**CG6707**	***CG6707***	**TMEM55B**
28	**CG17259**	***SerRS***	**SARS**	**78**	CG9423	*Kap-alpha3*	KPNA2	**128**	**CG4320**	***raptor***	**RPTOR**
29	CG8402	*PpD3*	PPP5C	**79**	CG10545	*Gbeta13F*	GNB4				
30	CG3616	*Cyp9c1*	CYP4F12	**80**	CG10913	*Spn55B*	SERPINB2				
31	CG5094	*Sgt*	SGTA	**81**	CG4265	*Uch*	UCHL3				
32	CG11015	*COX5B*	COX5B	**82**	CG3001	*Hex-A*	HK2				
33	**CG3595**	***sqh***	**MYL12B**	**83**	**CG8014**	***Rme-8***	**DNAJC13**				
34	CG6226	*FK506-bp1*	PPID	**84**	CG8683	*mon2*	MON2				
35	CG9881	*Arpc5*	ARPC5	**85**	CG17950	*HmgD*	SSRP1				
36	CG12108	*Ppt1*	PPT1	**86**	CG8284	*Ubc4*	UBE2K				
37	CG7619	*Rpn10*	PIP5K1C	**87**	CG12918	*sel*	CNPY1				
38	CG9281	*CG9281*	ABCF2	**88**	CG5252	*Ranbp9*	IPO9				
39	CG10425	*CG10425*	KDSR	**89**	CG8487	*garz*	GBF1				
40	CG13349	*Rpn13*	ADRM1	**90**	CG12132	*c11.1*	MROH7				
41	CG3226	*CG3226*	CACYBP	**91**	CG12065	*CG12065*					
42	CG34373	*Ect4*	SARM1	**92**	CG4225	*Hmt-1*	ABCB7				
43	CG16973	*msn*	TNIK	**93**	CG10161	*eIF-3p66*	EIF3D				
44	CG8251	*Pgi*	GPI	**94**	CG14616	*l(1)G0196*	PPIP5K1				
45	CG9242	*bur*	GMPS	**95**	CG42595	*uex*	CNNM2				
46	**CG13391**	***AlaRS***	**AARS**	**96**	CG3572	*vimar*	RAP1GDS1				
47	CG1691	*Imp*	IGF2BP3	**97**	CG11334	*CG11334*	MRI1				
48	CG6783	*fabp*	FABP2	**98**	CG4560	*Arpc3A*	ARPC3				
49	CG3593	*r-l*	UMPS	**99**	CG7806	*CG7806*	ABCC4				
50	**CG7891**	***Gie***	**ARL8B**	**100**	CG8715	*lig*	UBAP2				

Table 4. Enrichment analysis for Spg11 C-terminal interactors identified in both constitutive and inducible interaction screens.

GO term (cellular component)]	p-Value	Matches
cytoplasm [GO:0005737]	3.590803e-9	83
intracellular [GO:0005622]	7.562255e-8	103
proteasome regulatory particle [GO:0005838]	1.200421e-5	5
cytosol [GO:0005829]	1.404119e-5	31
proteasome accessory complex [GO:0022624]	1.459274e-5	5
fusome [GO:0045169]	3.470829e-5	5
actin cytoskeleton [GO:0015629]	3.953523e-5	8

Table 5. Members of the Sec1/Munc18 (SM) gene family in *Drosophila*

Gene Symbol	Gene Name	Also known as
car	*carnation*	*Vps33, Vps33a, l(1)G0447*
Rop	*Ras opposite*	*l(3)64Ah, cs1, Sec1, Munc18*
Slh	*SLY-1 homologous*	*Sly1, d-sly*
Vps33B	*Vacuolar protein sorting 33B*	
Vps45	*Vacuolar protein sorting 45*	*MEME(3R)-C*

Table 6. Rop, Vps45, Slh and Spg15 mass spectrometry score results

PMT-GFP::Spg11-C

Gene Symbol	Protein	CDS	Score	Matches	Sequences
Rop	CG15811	PA	180	3	3
Vps45	CG8228	PA	122	2	2
Slh	CG3539	PC	90	2	2
CG5270	CG5270	PB	63	1	1

Act5-GFP::Spg11-C

Gene Symbol	Protein	CDS	Score	Matches	Sequences
Rop	CG15811	PA	80	1	1

Table 7. MARS and AARS mass spectrometry results

PMT-GFP::Spg11-C

***Drosophila* Protein**	**Human Ortholog**	**CDS**	**Score**	**Matches**	**Sequences**
MetRS	MARS	PA	1147	26	14
SerRS	SARS	PA	341	6	4
AlaRS	AARS	PB	338	5	2
ValRS	VARS	PB	331	5	3
GlnRS	QARS	PA	125	4	3

Act5-GFP::Spg11-C

***Drosophila* Protein**	**Human Ortholog**	**CDS**	**Score**	**Matches**	**Sequences**
SerRS	SARS	PA	135	2	1
MetRS	MARS	PA	125	1	1